Gravitational wave emission from the bar-mode instability in core-collapse supernovae

Pablo Cerdá-Durán

October 11, 2021

1 Introduction

During previous targeted searches of GW signals from core-collapse supernovae (CCSNe) [Abbott et al., 2016, 2020] the collaboration has used some extreme emission models as a limit of plausible GW emission. One of the models, the so-called *long-lasting bar mode* model (long-bar hereafter), consists of a rotating cylinder [Ott, 2010] which mimics the presence of bar-mode instabilities in the proto-neutron star formed after the star has collapsed. As the sensitivity improves, this model has began to be tested and some constraints have been possible with the data of the O1-O2 run [Abbott et al., 2020]. Given that the sensitivity will increase in future runs and better constraints on the model are foreseeable, one should question if a cylindrical bar is the best possible model to describe bar-modes and if the constraints that we are getting on the parameters of the model (such as length, diameter and mass of the bar) are the more interesting ones from an observational perspective.

2 GW from rotating rigid bodies

The reduced mass quadrupole momentum is defined as [see e.g. Misner et al., 2017]

$$I_{ij} = \int dV \rho \left[x_i x_j - \frac{1}{3}\delta_{ij}(x_1^2 + x_2^2 + x_3^2) \right] \ . \tag{1}$$

where ρ is the rest mass density and $x_i \equiv \{x, y, x\}$ the Cartesian coordinates. In the quadrupolar approximation, the transverse-traceless (TT) GW signal is given by

$$h_{ij}^{TT} = \frac{2}{D}\frac{G}{c^4} P_{ij}{}^{kl} \ddot{I}_{kl} \ , \tag{2}$$

where $P_{ij}{}^{kl}$ is the TT projector operator and D the distance to the source.

If we consider a rigid body rotating around the z axis (no precession or nutation) with a rotational frequency $f_{\rm rot}$, the quadrupolar GW emission can be written, without loss of generality as [Zimmermann and Szedenits, 1979, Brady et al., 1998, Jaranowski et al., 1998]

$$h_+ = \frac{1}{2} h_0 \left(1 + \cos^2 i\right) \cos(2\pi f_0 t) \tag{3}$$

$$h_\times = h_0 \cos i \, \sin(2\pi f_0 t) \tag{4}$$

where i is the inclination angle of the observer with respect to the z axis, $f_0 = 2 f_{\rm rot}$ and

$$h_0 = \frac{2}{D}\frac{G}{c^4}\frac{I_{xx} - I_{yy}}{2}(2\pi f_0)^2. \tag{5}$$

We can particularise this expression to different rigid bodies.

2.1 Triaxial ellipsoid

If we consider a triaxial ellipsoid rotating about a principal axis then

$$h_0 = \frac{2}{D}\frac{G}{c^4}\frac{I_{zz}\epsilon}{2}(2\pi f_0)^2, \tag{6}$$

where the ellipticity is defined as

$$\epsilon \equiv \frac{I_{xx} - I_{yy}}{I_{zz}} \tag{7}$$

and is a measure of the deformation of the star. This approach has been used in searches for continuous GWs from isolated rotating neutron stars [Abbott et al., 2019a].

2.2 Rotating cylinder

In previous SN searches papers [Abbott et al., 2016, 2020] we have considered a spinning cylinder [Ott, 2010], with radius R, length L and mass M. In this case

$$I_{xx} = \frac{1}{12}M(3R^2 + L^2), \tag{8}$$

$$I_{yy} = \frac{1}{2}MR^2, \tag{9}$$

$$I_{zz} = \frac{1}{12}M(3R^2 + L^2), \tag{10}$$

i.e.

$$I_{xx} - I_{yy} = \frac{1}{12}M(L^2 - 3R^2), \tag{11}$$

and therefore

$$h_0 = \frac{2}{D}\frac{G}{c^4}\frac{1}{6}M(L^2 - 3R^2)(2\pi f_{\rm rot})^2 = \frac{2}{D}\frac{G}{c^4}\frac{1}{24}M(L^2 - 3R^2)(2\pi f_0)^2 \tag{12}$$

Note that the case of the rotating cylinder can also be written in terms of ellipticity considering

$$\epsilon = \frac{L^2 - 3R^2}{L^2 + 3R^2}. \tag{13}$$

In this case, the zero-ellipticity limit corresponds to

$$L = \sqrt{3}R = \frac{\sqrt{3}}{2}(2R) \approx 0.866(2R). \tag{14}$$

A cylinder with this particular length-to-radius ratio should not emit any gravitational wave.

3 Motivation

From the perspective of GW detection any rotating rigid body will emit the same GW signal provided they have the same $I_{yy} - I_{xx}$ and have the same inclination i and distance D. Therefore the shape of the rigid body that we consider for our model of the bar mode should be irrelevant.

However, the interpretation of the results depends on the model used. SN searches during the previous GW observational campaigns have allowed to put constraints for the first time on the amplitude of the waveform h_0, or if one considers the distance known, in the combination $I_{yy} - I_{xx}$. However, we have interpreted this result using a particular model (cylindrical bar) and tried to put constraints in the parameter space formed by M, L and R. The use of this particular model has several problems:

- The shape of a cylindrical bar do not resemble the shape of the bar (actually an l=2 mode) developing in the proto-neutron star; it is actually more similar to a triaxial ellipsoid.
- As detectors improve we will put better constraints on $I_{yy} - I_{xx}$. At some point we will be in a regime in which our constrain is sufficiently small such that we are in the regimen in which $L \sim \sqrt{R}$. At this point it will become very difficult to interpret the system as a cylindrical bar. It would be much more appropriate the use of the ellipticity ϵ, that will go smoothly to zero as we improve our sensitivity (or make a detection).
- Cylinders with length $L < \sqrt{3}R$ have negative ellipticity, which corresponds to an oblate ellipsoid rotating with respect to an axis perpendicular to the symmetry axis (like a spinning coin). This case is not relevant for the case of the bar-mode instability.

As a conclusion, I suggest the use of a triaxial ellipsoids as a model for the bar mode instability. The advantages are:

- We can perform a series of simulations with constant f_0 and several values of ϵI_{zz}. The result will put an upper limit on the acceptable value for ϵI_{zz}. The range of values can be extended towards zero as we increase sensitivity.
- This approach is backwards compatible with previous results, because the limit on ϵI_{zz} can be computed in terms of the limits for the cylinder that we found in previous searches.
- We do not need any new development or implementation to perform the analysis. We can use the already available pipelines and reinterpret all the results in terms of ϵI_{zz}.
- There is plenty of literature on the momentum of inertia of neutron stars (I_{zz}) both from the theoretical and observational perspective (pulsar spin-down, glitches ...). Using the existing constraints for I_{zz} it is possible to put constraints to ϵ, which is a direct measurement of deformation of the proto-neutron star. We can use a canonical value of the moment of inertia of neutron stars of $I_{zz} = 10^{45}$ g cm^2, similarly to Abbott et al. [2019a].

Ranges for the possible values of I_{zz} and ϵ could be easily provided if the collaboration thinks this is the appropriate approach for the next observing runs.

4 Waveforms

4.1 Previously used long-bar waveforms

The waveforms previously used for the bar-mode are described in Ott [2010] and the companion python code bargw.py (`https://dcc.ligo.org/LIGO-T1000553/public`). A more detailed description of the waveforms can be found in Gossan et al. [2016a]. The waveforms consist essentially of the the waveform described in section 2.2 windowed by a Gaussian profile of width $\tau = \Delta t/4$, being Δt the duration of the signal. Some comments should be made about the waveforms:

- The explicit expressions for h_+ and $h_\times$ that can be derived from [Ott, 2010] are wrong in a "$-$" sign in $h_\times$. This probably comes from a wrong sign in Eq. (6) of this work ($\sin 2\Omega t \rightarrow -\sin 2\Omega t$). This sign differs from the expressions found in Zimmermann and Szedenits [1979], Brady et al. [1998], Jaranowski et al. [1998]. However, the results are correct if one considers that the bar is rotating clockwise instead of counterclockwise.
- The output of bargw.py is the real and imaginary part of h, not $h_+ = Re(h)$ and $h_\times = -Im(h)$ (note the missing "$-$" in $h_\times$). For $\varphi = \theta = 0$ it can be easily checked that the result from the python script does not result in Eqs. (16-17) in [Ott, 2010]. The results of the script are actually consistent with making the transformation $\Omega \rightarrow -\Omega$, which compensates the error in the expressions in [Ott, 2010]

- bargw.py has a bug in the implemented expression for ${}^{-2}Y_{2\pm1}$, it contains the term $\sin\theta + (1+\cos\theta)$ but it should be $\sin\theta(1+\cos\theta)$ according to [Ott, 2010]. The bug does not affect the computation because the coefficient multiplying this spherical harmonic is $H^{\rm quad}_{2\pm1} = 0$.

- The shape of the Gaussian window is not described in [Ott, 2010]. The window implemented in bargw.py is

$$\exp\left(-\frac{(t-\Delta t/2)^2}{\tau^2}\right). \tag{15}$$

  However, in [Gossan et al., 2016b] the window is

$$\exp\left(-\frac{(t-\Delta t)^2}{\tau^2}\right). \tag{16}$$

  As we show below this time shift is not relevant for the analysis as long as $2\pi f_0\tau >> 1$, which is always the case.

As a result, despite of the errors in [Ott, 2010] and bargw.py, which compensate each other, the numerical output of the code is correct.

4.2 Ad-hoc waveforms

Previous all-sky burst searches Abadie et al. [2012], Abbott et al. [2019b] and supernova searches [Abbott et al., 2016, 2020] have used sine-Gaussian waveforms as a model for unmodeled burst. According to Abadie et al. [2012]

$$h_+(t) = \frac{1}{2}A\,(1+\alpha^2)\,\exp\left(-\frac{t^2}{\tau^2}\right)\sin(2\pi f_0 t + \varphi), \tag{17}$$

$$h_\times(t) = A\alpha\exp\left(-\frac{t^2}{\tau^2}\right)\cos(2\pi f_0 t + \varphi), \tag{18}$$

where A is the amplitude, τ is related to the duration and f_0 the observed frequency. α is the waveform ellipticity (do not confuse with the neutron star ellipticity, ϵ). α can take values in the interval $[0,1]$, where $\alpha = 0$ corresponds to linearly polarised waves and $\alpha = 1$ to circular polarised waves. φ is an arbitrary phase that we use to encapsulate the different definitions used by different authors. In particular for [Ott, 2010] its value is $\varphi = 4\pi f_0\tau$ and for [Gossan et al., 2016b] is $\varphi = 8\pi f_0\tau$.

The functional form of this expression is identical to the waveform of a triaxial ellipsoid or a rotating cylinder given by Eqs. (3)and (4) making the next identifications

- $A = h_0$
- Add a phase $+\pi/2$ to the harmonic dependence
- $f_0 \to -f_0$
- $\alpha = \cos i$

In order to recover the results of bargw.py there is an additional phase $+\pi$ (i.e. a global "$-$" sign in h).

As a conclusion long-bar and sine-Gaussian waveforms are identical and should not be necessary to use two different kind of waveforms in any analysis.

Table 1: Correspondence between the long-bar models, the triaxial ellipsoid model and the sine-Gaussian parametrisation. We consider a source at a distance $D = 10$ kpc. There is an additional $\pi/2$ phase difference between models, irrelevant for this work. Note that τ may be wrong by a factor 4 (see comments in text).

	long-bar/triaxial ellipsoid parameters							sine-Gaussian parameters			
Model	M	L	R	$f_{\rm rot}$	Δt	$\cos i$	$I_{zz}\epsilon$	h_0	f_0	τ	α
	$[M_\odot]$	[km]	[km]	[Hz]	[ms]		$[10^{45}$ g cm$^2]$	$[10^{-19}]$	[Hz]	[ms]	
lb1	0.2	60	10	400	100	$[0,1]$	1.09	0.74	-800	25	$[0,1]$
lb2	0.2	60	10	400	1000	$[0,1]$	1.09	0.74	-800	250	$[0,1]$
lb3	0.2	60	10	800	100	$[0,1]$	1.09	2.96	-1600	25	$[0,1]$
lb4	1.0	60	10	400	100	$[0,1]$	5.47	3.70	-800	25	$[0,1]$
lb5	1.0	60	10	400	1000	$[0,1]$	5.47	3.70	-800	250	$[0,1]$
lb6	1.0	60	10	800	25	$[0,1]$	5.47	14.8	-1600	6.25	$[0,1]$

4.3 New waveforms

We propose to use the sine-Gaussian waveforms, Eqs. (17)-(18), to describe long-bar waveforms with the next parametrisation:

$$A = h_0 = \frac{2}{D}\frac{G}{c^4}\frac{I_{zz}\epsilon}{2}(4\pi f_{\rm rot})^2, \tag{19}$$

$$\alpha = \cos i, \tag{20}$$

$$f_0 = -2f_{\rm rot}. \tag{21}$$

To simplify we do not correct for the $\pi/2$ phase difference, because corresponds to an arbitrary initial phase and because is likely irrelevant for burst searches. In Table 1 we show the correspondence between the long-bar models and sine-Gaussians in Abbott et al. [2016, 2020]. Note that the values for Δt are those given for the duration of the waveform in Abbott et al. [2016, 2020] and τ should be 1/4th of that values. However, the $h_{\rm rss}$ values in table IV of Abbott et al. [2020] are only obtained if duration is interpreted as τ directly. In any case, factor does not affects the calculations of the next section since the factors cancel out.

It is possible to compute analytically the angle-averaged rss value of h as (see the Mathematica notebook hrss.nb):

$$h_{\rm rss} \equiv \sqrt{\int < h_+^2(t) + h_\times^2(t) >_\Omega dt} = A\left(\frac{\pi}{2}\right)^{1/4}\sqrt{\frac{6\tau}{15}}\sqrt{1 - \frac{\cos(2\varphi)}{6}e^{-(2\pi f_0\tau)^2/2}} \tag{22}$$

where we have performed the time integral in the interval $[-\infty, \infty]$, and the angular average corresponds to an average on α in the range $[-1, 1]$. The last term can be neglected if $2\pi f_0\tau >> 1$, which will be in all the cases considered, so the result does not depend on the arbitrary phase:

$$h_{\rm rss} \approx A\left(\frac{\pi}{2}\right)^{1/4}\sqrt{\frac{6\tau}{15}} \approx 0.708A\sqrt{\tau} \tag{23}$$

If we make the time integral using the duration of the signal $[-\Delta t/2, \Delta t/2]$ instead, the result barely changes (difference in the 5th significant digit).

5 Re-interpretation of O1+O2 results

Using this new framework we can re-interpret the results of the O1+O2 search for SNe reported in Abbott et al. [2020] in terms of ellipticity. All the computations can be found in long-bar_estimates.ipynb. Here we just summarise the final results. Fig. 1 shows the upper limits for

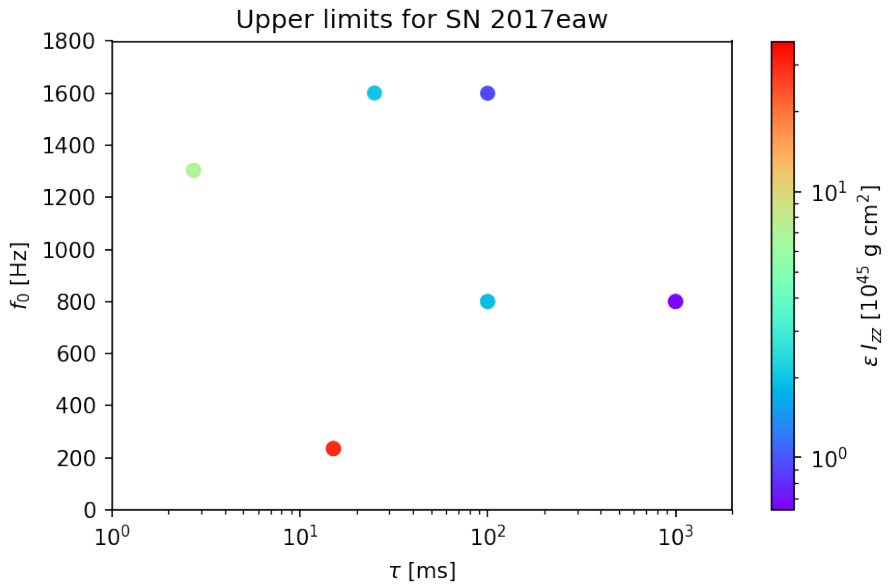

Figure 1: Upper limits for SN 2017eaw (the closest event in the sample) on the value of ϵI_{zz} depending on the observed frequency f_0 and the parameter τ controlling duration of the signal.

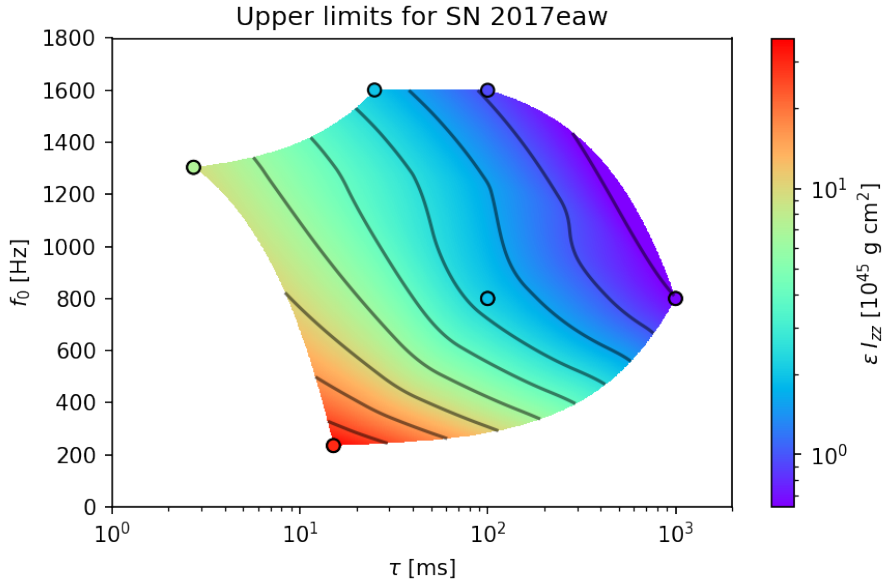

Figure 2: Same as Fig 1 but including interpolated values (color coded and contours) within the parameter space explored.

SN 2017eaw on the value of ϵI_{zz} depending on f_0 and τ. This is the closest event in the sample (6.72 Mpc), for which we have the most constraining upper limits. Note that since it is expressed in units of 10^{45} g cm^2, the canonical value of the momentum of inertia of neutron stars, it can be directly read as an estimation of the upper limit of the ellipticity ϵ. Fig. 2 is a similar plot with the addition of of interpolated values between the few scattered plots to better show the dependence. Details on how the interpolation is done can be found in longbar_estimates.ipynb. For future searches, a more evenly spaced and denser grid of points could be done so that we have better estimates of the constraints in the f_0-τ plane.

The results show that we either had a long duration-high frequency signal with $\epsilon I_{zz} \lesssim 1$ or a short duration-low frequency signal with $\epsilon I_{zz} \lesssim 100$. This dependence can be undertood in terms of the different parameters since the upper limits are

- proportional to $1/f_0$, because of the shape of the sensitivity curves at high frequencies dominated by shot-noise; the ASD of the noise is proportional to f_0 and at the same time $h_{\rm rss}$ of the signal is proportional to f_0^2.
- proportional to $1/\sqrt{\tau}$, because of the dependence of $h_{\rm rss}$ on $\sqrt{\tau}$ (see Eq. (23)).
- proportional to D, because of the dependence of the wave amplitude on D.

This dependence allow us to make an average over all the constraints for all the SNe observed that results in the next upper limits

$$\epsilon = (1.6 \pm 0.6) \left(\frac{10^{45}\,\mathrm{g\,cm^2}}{I_{zz}}\right) \left(\frac{1000\,\mathrm{Hz}}{f_0}\right) \sqrt{\frac{0.1\,\mathrm{s}}{\tau}} \left(\frac{D}{6\,\mathrm{Mpc}}\right) \tag{24}$$

where the error bar corresponds to the standard deviation.

For a galactic supernova, at a distance about 1000 times closer that the event considered here, we expect to be sensitive to values 1000 smaller, in the range of predictions for magneto-rotational explosions.

6 Parameter space

For future searches we have to find ways to sample properly the f_0-τ plane. We can have some estimates on the limits by looking at numerical simulations of CCSN that show signatures of bar mode instabilities. Table 2 shows the typical values found in numerical simulations compared with the ones used for the O1-O2 search and the proposal for O3.

References

J. Abadie, B. P. Abbott, R. Abbott, T. D. Abbott, M. Abernathy, T. Accadia, F. Acernese, C. Adams, R. Adhikari, C. Affeldt, and et al. All-sky search for gravitational-wave bursts in the second joint LIGO-Virgo run. Phys. Rev. D, 85(12):122007, June 2012. doi: 10.1103/PhysRevD.85.122007.

B. P. Abbott, R. Abbott, T. D. Abbott, M. R. Abernathy, F. Acernese, K. Ackley, C. Adams, T. Adams, P. Addesso, R. X. Adhikari, and et al. First targeted search for gravitational-wave bursts from core-collapse supernovae in data of first-generation laser interferometer detectors. Phys. Rev. D, 94(10):102001, November 2016. doi: 10.1103/PhysRevD.94.102001.

B. P. Abbott, R. Abbott, T. D. Abbott, S. Abraham, F. Acernese, K. Ackley, C. Adams, R. X. Adhikari, V. B. Adya, C. Affeldt, and et al. All-sky search for continuous gravitational waves from isolated neutron stars using Advanced LIGO O2 data. Phys. Rev. D, 100(2):024004, July 2019a. doi: 10.1103/PhysRevD.100.024004.

Table 2: Summary of the results of previous simulations on non-axisymmetric instabilities in core-collapse supernovae. h_max refers to the amplitude for the most extreme simulation in each work. Last row is the range used previous SN searches and the constraints set by the non-observation.

Work	Gravity	EOS	$f_{\rm GW}$[Hz]	$Dh_{\rm max}$[cm]	T[ms]	notes
Rampp et al. [1998]	Newt.	Hybrid	-	500	> 10	
Shibata and Sekiguchi [2005]	GR	Hybrid	~ 1000	10^4	~ 2	
Ott et al. [2005]	Newt.	Ideal fluid	~ 800	100	$10 - 50$	
Ott et al. [2007]	GR	Shen	930	700	> 30	
Scheidegger et al. [2008]	Newt. 1D	LS	905	50	> 20	
Scheidegger et al. [2010]	TOV 1D	Shen/LS	$662 - 935$	$50 - 100$	$> 30 - 200$	
Kuroda et al. [2014]	GR	Shen	$700 - 1000$	20	8	after bounce
			$100 - 200$		> 20	later phase
Takiwaki and Kotake [2018]	Newt. 1D	LS220	240	30	> 200	
Shibagaki et al. [2020]	GR	LS220	400	~ 300	20	at 80ms p.b.
			$400 - 800$	~ 300	> 200	from 120ms p.b.
Pan et al. [2020]	TOV	LS220	$450 - 800$	~ 300	200	
O1+O2 search			$800 - 1600$	< 5700	$25 - 1000$	lb models
			$235 - 1304$	$< 10^4 - 10^5$	$(2.7 - 15.1) \times 4$	sg models
O3 proposal			$50 - 1500$		$1 - 1000$	sg models (5x5)

B. P. Abbott, R. Abbott, T. D. Abbott, S. Abraham, F. Acernese, K. Ackley, C. Adams, R. X. Adhikari, V. B. Adya, C. Affeldt, and et al. All-sky search for short gravitational-wave bursts in the second Advanced LIGO and Advanced Virgo run. Phys. Rev. D, 100(2):024017, July 2019b. doi: 10.1103/PhysRevD.100.024017.

B. P. Abbott, R. Abbott, T. D. Abbott, S. Abraham, F. Acernese, K. Ackley, C. Adams, V. B. Adya, C. Affeldt, M. Agathos, and et al. Optically targeted search for gravitational waves emitted by core-collapse supernovae during the first and second observing runs of advanced LIGO and advanced Virgo. Phys. Rev. D, 101(8):084002, April 2020. doi: 10.1103/PhysRevD.101.084002.

Patrick R. Brady, Teviet Creighton, Curt Cutler, and Bernard F. Schutz. Searching for periodic sources with LIGO. Phys. Rev. D, 57(4):2101–2116, February 1998. doi: 10.1103/PhysRevD.57.2101.

S. E. Gossan, P. Sutton, A. Stuver, M. Zanolin, K. Gill, and C. D. Ott. Observing gravitational waves from core-collapse supernovae in the advanced detector era. Phys. Rev. D, 93(4):042002, February 2016a. doi: 10.1103/PhysRevD.93.042002.

S. E. Gossan, P. Sutton, A. Stuver, M. Zanolin, K. Gill, and C. D. Ott. Observing gravitational waves from core-collapse supernovae in the advanced detector era. Phys. Rev. D, 93(4):042002, Feb 2016b. doi: 10.1103/PhysRevD.93.042002.

Piotr Jaranowski, Andrzej Królak, and Bernard F. Schutz. Data analysis of gravitational-wave signals from spinning neutron stars: The signal and its detection. Phys. Rev. D, 58(6):063001, September 1998. doi: 10.1103/PhysRevD.58.063001.

Takami Kuroda, Tomoya Takiwaki, and Kei Kotake. Gravitational wave signatures from low-mode spiral instabilities in rapidly rotating supernova cores. Phys. Rev. D, 89(4):044011, February 2014. doi: 10.1103/PhysRevD.89.044011.

Charles W. Misner, Kip S. Thorne, and John Archibald Wheeler. Gravitation. 2017.

C. D. Ott, H. Dimmelmeier, A. Marek, H. T. Janka, I. Hawke, B. Zink, and E. Schnetter. 3D Collapse of Rotating Stellar Iron Cores in General Relativity Including Deleptonization and a Nuclear Equation of State. Phys. Rev. Lett., 98(26):261101, June 2007. doi: 10.1103/PhysRevLett.98.261101.

C.D. Ott. Lvc technical report ligo-t1000553-v1. Technical report, LVC, 2010.

Christian D. Ott, Shangli Ou, Joel E. Tohline, and Adam Burrows. One-armed Spiral Instability in a Low-T/—W— Postbounce Supernova Core. ApJ, 625(2):L119–L122, June 2005. doi: 10.1086/431305.

Kuo-Chuan Pan, Matthias Liebendörfer, Sean Couch, and Friedrich-Karl Thielemann. Stellar Mass Black Hole Formation and Multi-messenger Signals from Three Dimensional Rotating Core-Collapse Supernova Simulations. arXiv e-prints, art. arXiv:2010.02453, October 2020.

M. Rampp, E. Mueller, and M. Ruffert. Simulations of non-axisymmetric rotational core collapse. A&A, 332:969–983, April 1998.

S. Scheidegger, T. Fischer, S. C. Whitehouse, and M. Liebendörfer. Gravitational waves from 3D MHD core collapse simulations. A&A, 490(1):231–241, October 2008. doi: 10.1051/0004-6361:20078577.

S. Scheidegger, R. Käppeli, S. C. Whitehouse, T. Fischer, and M. Liebendörfer. The influence of model parameters on the prediction of gravitational wave signals from stellar core collapse. A&A, 514:A51, May 2010. doi: 10.1051/0004-6361/200913220.

Shota Shibagaki, Takami Kuroda, Kei Kotake, and Tomoya Takiwaki. A new gravitational-wave signature of low-T/—W— instability in rapidly rotating stellar core collapse. MNRAS, 493(1): L138–L142, March 2020. doi: 10.1093/mnrasl/slaa021.

Masaru Shibata and Yu-Ichirou Sekiguchi. Three-dimensional simulations of stellar core collapse in full general relativity: Nonaxisymmetric dynamical instabilities. Phys. Rev. D, 71(2):024014, January 2005. doi: 10.1103/PhysRevD.71.024014.

Tomoya Takiwaki and Kei Kotake. Anisotropic emission of neutrino and gravitational-wave signals from rapidly rotating core-collapse supernovae. MNRAS, 475(1):L91–L95, March 2018. doi: 10.1093/mnrasl/sly008.

M. Zimmermann and Jr. Szedenits, E. Gravitational waves from rotating and precessing rigid bodies: Simple models and applications to pulsars. Phys. Rev. D, 20(2):351–355, July 1979. doi: 10.1103/PhysRevD.20.351.